INTERNATIONAL JOURNAL FOR NUMERICAL METHODS IN FLUIDS
*Int. J. Numer. Meth. Fluids* 2002; **40**:379–389 (DOI: 10.1002/fld.293)

# Vortex structure and strength of secondary flows in model aortic arches

San-Yih Lin* and Zhong-Xin Yu

*Department of Aeronautics and Astronautics, National Cheng Kung University Tainan, Taiwan, R.O.C.*

SUMMARY

A numerical method is developed to study the flow structures in the aortic arch. The method solves the incompressible Navier–Stokes equations. It uses a third-order upwind scheme for the convective terms and the second-order central scheme for the viscous terms. A DDADI time integration is used for achieving fast convergence. For the unsteady solutions, the second-order Crank–Nicolson method coupled with the diagonalized diagonal dominated alternating direction implicit scheme (DDADI) time integration are used. The numerical results show that the method is about 2.5-order accuracy in space and 1.8-order accuracy in time. Then the method is used to investigate the vortex structure and strength of secondary flows in the aortic arch. Four different arch geometries are constructed to see the effect of arch configuration. Many flow properties such as pressure drop, vortex strength and separation are computed and compared among the four arch models. Copyright © 2002 John Wiley & Sons, Ltd.

KEY WORDS: aortic Arch; DDADI; incompressible flow; Crank–Nicolson method; secondary flow

## 1. INTRODUCTION

The flow round the aortic arch is important research subject recently [1, 2]. Secondary flow patterns associated with the generation and transport of vortices will be a fundamental subject. It is well known that two counter-rotating vortices are generated when fluid flows around a single bend. Kilner *et al.* [2] presented the secondary flows and the helical flow pattern by using magnetic resonance mapping techniques. Black *et al.* [3] studied these phenomena by using computational fluid dynamics. They found that an additional bend in the flow path could initiate changes on vortex structure and proposed a Kilner's arch which can change the normal double-vortices pattern to the single helical flow pattern. In this paper, four different parametric models of the aortic arch are constructed to see the effect of arch configuration. Many flow properties such as pressure drop, vortex strength, and separation are computed and compared among the four arch models. Numerical solutions to the incompressible Navier–

*Correspondence to: S.-Y. Lin, Department of Aeronautics and Astronautics, National Cheng Kung University, Taiwan, R.O.C.

Contract/grant sponsor: National Science Council, Republic of China; contract/grant number: NSC 89-2212-E-006-191

*Received May 2001*
*Revised September 2001*

Stokes equations are in greater demand than ever before as the field of computational fluid dynamics increases its importance as an engineering tool. An efficient code is a key to be a useful tool for flow analysis. Therefore, there is a continuing interest in finding solution methodologies which will produce results using the least amount of computing time and CPU memories. This is particularly true for problems with a high Reynolds number. In this paper, the proposed numerical method is based on an artificial compressibility approach which has been used successfully by a number of other authors [4–6]. The advantages of using artificial compressibility are that it directly couples the pressure and velocity fields at the same time level and produces a hyperbolic-dominated system of equations. Since the equations are hyperbolic dominated, some of the upwind finite-volume schemes which have recently been developed for the compressible Euler and Navier–Stokes equations can be utilized. For the time integration, the second-order Crank–Nicolson method coupled with a DDADI time integration [7] is used. In the following sections, the details of the artificial compressibility method and its applications in solving the incompressible Navier–Stokes equation for both steady-state and unsteady problems are given. First a comparison with an analytical solution is performed to show the space and time accuracy of the method. Then, the flow structures in the aortic arch are investigated.

## 2. NUMERICAL FORMULATION

### 2.1. Governing equations and artificial compressibility method

The conservative form of the steady incompressible Navier–Stokes equations with artificial compressibility parameter is following:

$$\frac{\partial}{\partial t}Q + \nabla \cdot (F, G, H) = \frac{1}{Re}\Delta\phi \tag{2.1}$$

where

$$Q = \begin{pmatrix} p \\ u \\ v \\ w \end{pmatrix}, \quad F = \begin{pmatrix} \beta u \\ u^2 + p \\ uv \\ uw \end{pmatrix}, \quad G = \begin{pmatrix} \beta v \\ uv \\ v^2 + p \\ vw \end{pmatrix}, \quad H = \begin{pmatrix} \beta w \\ uw \\ vw \\ w^2 + p \end{pmatrix}, \quad \phi = \begin{pmatrix} 0 \\ u \\ v \\ w \end{pmatrix}$$

$p$ and $(u, v, w)$ are the pressure, the Cartesian velocity $\beta$, $\beta > 0$ is the artificial compressibility parameter and $Re$ is the Reynolds number corresponding to the free-stream velocity. The steady-state solution of Equation (2.1) achieves divergence-free flow.

### 2.2. Space discretization: finite-volume formulation

Let the three-dimensional computational domain be discretized into a group of hexahedrons $K_{ijk}$. In each hexahedron $K_{ijk}$, flow variables are stored at the barycentre $C_{ijk}$ and the flow conservation is enforced on the boundary surface $\Gamma_{i,j,k}$. The integral form of Equation (2.1) can be written as

$$\frac{\mathrm{d}Q_{ijk}}{\mathrm{d}t} = -\frac{1}{V_{ijk}}\left(\int\int_{\Gamma}(E, F, G)\cdot\mathbf{n}\,\mathrm{d}A + \frac{1}{Re}\int\int_{\Gamma}(\nabla\phi)\cdot\mathbf{n}\,\mathrm{d}A\right) \tag{2.2}$$

 

where $V_{ijk}$ is the volume of $K_{ijk}$. To evaluate the first term of the right-hand side of (2.2), we sum all the flux vectors on the six boundary surfaces of $K_{ijk}$.

$$\begin{aligned}\int_\Gamma (F,G,H)\cdot\mathbf{n}\,\mathrm{d}A = {} & h_{i-1/2,j,k}|s_{i-1/2,j,k}| + h_{i+1/2,j,k}|s_{i+1/2,j,k}| \\ & + h_{i,j-1/2,k}|s_{i,j-1/2,k}| + h_{i,j+1/2,k}|s_{i,j+1/2,k}| \\ & + h_{i,j,k-1/2}|s_{i,j,k-1/2}| + h_{i,j,k+1/2}|s_{i,j,k+1/2}|\end{aligned}$$

where $h_{i+1/2,jk}$ is the numerical approximation for the flux associated with the interface $A_{i+1/2,jk}$ and $|s_{i+1/2,jk}|$ is the area of the surface $A_{i+1/2,jk}$. In order to evaluate $h_{i+1/2,jk}$ using an upwind scheme, it is necessary to have two fluid dynamic states $Q^L_{i+1/2}$ and $Q^R_{i+1/2}$ (here, for simplicity, the notation $jk$ is neglected). The states $Q^L_{i+1/2}$ and $Q^R_{i+1/2}$ are interpolated from the cell centred states by means of a third-order partial-upwind scheme [6, 8]. Then the numerical flux at the interface $A_{i+1/2,j,k}$ is written as

$$\begin{aligned}h_{i+1/2} = h(Q^R_{i+1/2}, Q^L_{i+1/2}) = \frac{1}{2}[ & F(Q^R_{i+1/2})\cdot n_x + G(Q^L_{i+1/2})\cdot n_y \\ & + H(Q^R_{i+1/2})\cdot n_z + F(Q^L_{i+1/2})\cdot n_x \\ & + G(Q^R_{i+1/2})\cdot n_y + H(Q^L_{i+1/2})\cdot n_z \\ & - \alpha_{i+1/2}\cdot(Q^R_{i+1/2} - Q^L_{i+1/2})]\end{aligned} \tag{2.3}$$

Here the $(n_x, n_y, n_z)$ is the outer unit normal at the interface. the value $\alpha_{i+1/2}$ is defined as: $\alpha_{i+1/2} = \max(|U^L_n|, |U^R_n|)$ where $U_n = u_{i+1/2}\cdot n_x + v_{i+1/2}\cdot n_y + w_{i+1/2}\cdot n_z$ is the contravariant velocity normal to the surface $A_{i+1/2}$. The viscous terms are also computed by using a second-order finite-volume discretizations. Since the viscous flux components are functions of the velocity gradients, the divergence theorem is used to estimate appropriate values of these gradients on the cell faces [8].

### *2.3. Time integrations: DDADI algorithm and Crank–Nicolson method*

An implicit DDADI algorithm [7] is used to discretize the remaining time derivative in Equation (2.2). Define a residual as

$$\mathrm{Res}_{ijk} = \frac{1}{V_{ijk}}\int\!\!\int_\Gamma (F,G,H)\cdot\mathbf{n}\,\mathrm{d}A + \frac{1}{Re_\infty}\int\!\!\int_\Gamma (\nabla\phi)\cdot\mathbf{n}\,\mathrm{d}A$$

then, Equation (2.2) becomes

$$\mathrm{d}Q/\mathrm{d}t = \mathrm{Res}_{ijk} \tag{2.4}$$

Let $\Delta Q^n = Q^{n+1} - Q^n$. Using the two time-level scheme, Equation (2.4) can be solved as

$$\Delta Q^n = \Delta t[2\mathrm{Res}^{n+1} - \mathrm{Res}^n]$$

 

By Taylor expansion, Equation (2.4) can be solved by

$$[1 - 2(\partial \mathrm{Res}/\partial Q)^n \Delta t]\Delta Q^n = \mathrm{Res}^n$$

Finally use the DDADI scheme to solve $\Delta Q^n$ and set $Q^{n+1} = Q^n + \Delta Q^n$. The procedure converges up to almost divergence-free velocity fields. For the unsteady solutions, the unsteady Navier–Stokes equations is discretized by the second-order Crank–Nicolson method. Then the artificial compressibility method coupled with the DDADI algorithm is used to solve the solutions.

## 3. NUMERICAL TEST

The accuracy of the present method have been evaluated by solving a test problem for which the analytical solutions are available as functions of time, space, and Reynolds number. The solutions of the unsteady flow are given by the following Equations [9]:

$$\begin{aligned}
u &= -a[e^{ax}\sin(ay - dz) + e^{az}\cos(ax - dy)]e^{-d^2 t/Re} \\
v &= -a[e^{ay}\sin(az - dx) + e^{ax}\cos(ay - dz)]e^{-d^2 t/Re} \\
w &= -a[e^{az}\sin(ax - dy) + e^{ay}\cos(az - dx)]e^{-d^2 t/Re} \\
p &= -a^2\frac{1}{2}[e^{2ax} + e^{2ay} + e^{2az} + 2\sin(ax - dy)\cos(az - dx)e^{a(y+z)} \\
&\quad + 2\sin(ay - dz)\cos(ax - dy)e^{a(x+y)}]e^{-2d^2 t/Re}
\end{aligned}$$

here $a = \pi/4$, $d = \pi/2$ and $Re = 100$. The Navier–Stokes equations are solved numerically by the present method in the cubic domain, $[-1, 1]^3$. The computational domain is divided by $N$ uniform meshes. Table I shows the spatial errors ($L_2$ norm) of pressure and velocity fields at time, $T = 0.1$. The overall order of accuracy in space is around 2.5. Table II shows the

Table I. Spatial errors of pressure and velocity fields.

| $N$ | $P$ | Order | $U$ | Order |
|---|---|---|---|---|
| 8 | 1.5E-3 | | 1.4E-3 | |
| 16 | 2.7E-4 | 2.5 | 2.4E-4 | 2.6 |
| 24 | 9.2E-5 | 2.6 | 1.4E-3 | 2.6 |
| 32 | 4.2E-5 | 2.6 | 3.8E-5 | 2.6 |

Table II. Temporal errors of pressure and velocity fields.

| $\Delta t$ | $P$ | Order | $U$ | Order |
|---|---|---|---|---|
| 1.2 | 5.2E-3 | | 5.6E-3 | |
| 0.6 | 1.3E-3 | 1.9 | 1.5E-3 | 1.9 |
| 0.4 | 7.6E-4 | 1.7 | 7.4E-4 | 1.8 |

 

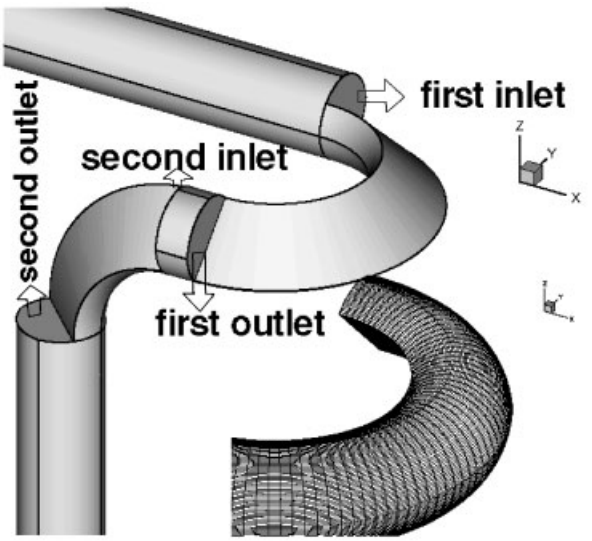


Figure 1. The positions of first inlet, first outlet, second inlet, and second outlet of the Kilner arch.

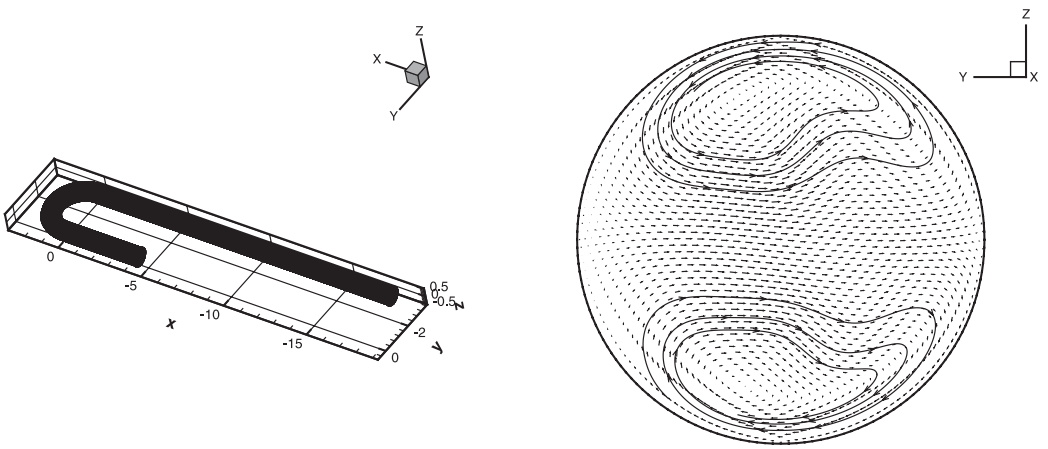


(a) (b)

Figure 2. (a) Grid of plane arch. (b) Velocity distribution at the first outlet.

temporal errors of pressure and velocity fields at time, $T = 4.8$. It is about 1.8-order accuracy in time.

## 4. RESULT AND DISCUSSION

In this section, the flows in the aortic arches under $Re = 1000$ are investigated. Secondary flow patterns associated with the generation and transport of vortices are the main subjects.

 

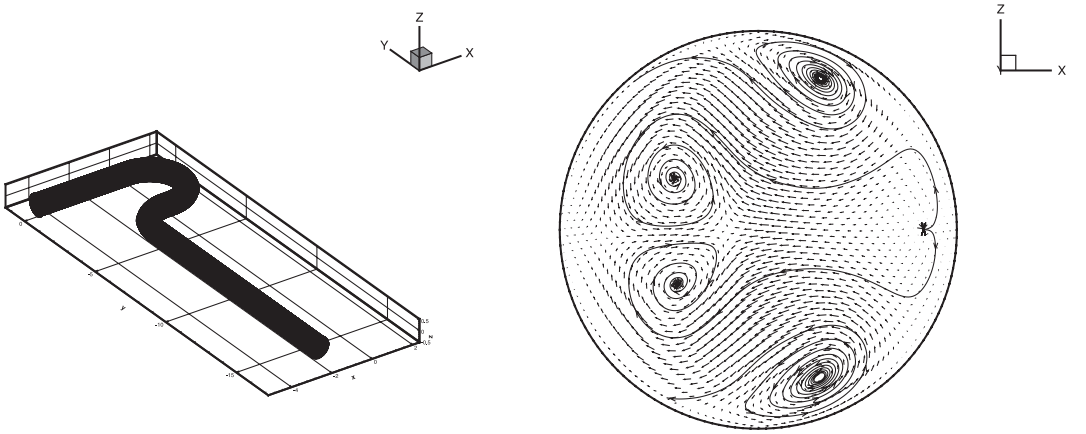


(a) (b)

Figure 3. (a) Grid of bi-curved arch. (b) Velocity distribution at the second outlet.

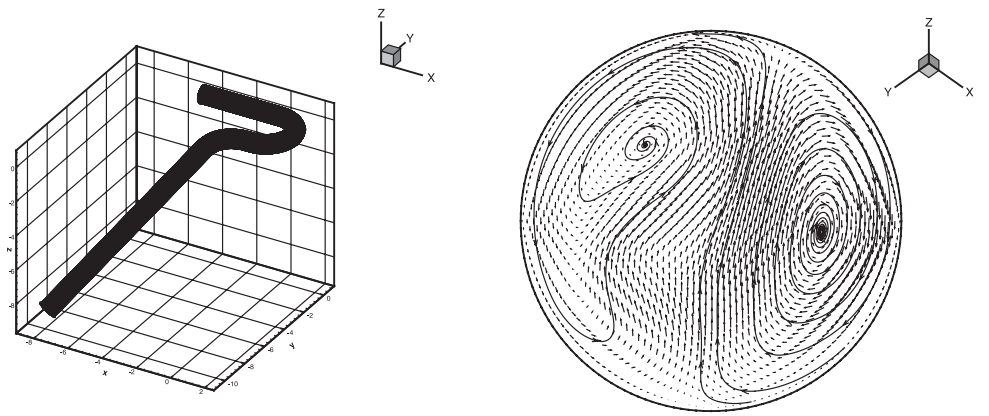


(a) (b)

Figure 4. (a) Grid of 45° arch. (b) Velocity distribution at the second outlet.

Four different arch geometries are constructed. Grid numbers of these four cases are $160 \times 40 \times 40$:

(1) Plane arch, featuring a arch with the axis curved in one plane.
(2) Bi-curved plane arch, featuring a similar tube with one more 90° turning in the same plane.
(3) 45° arch, featuring a plane arch a 45° out-of-plane inlet section.
(4) 90° arch (Kilner model), featuring a plane arch with a 90° out of plane inlet section. The helical flow pattern is the main vortex structure for this model. Figure 1 indicates the positions of first inlet, first outlet, second inlet, and second outlet of the arch.

 

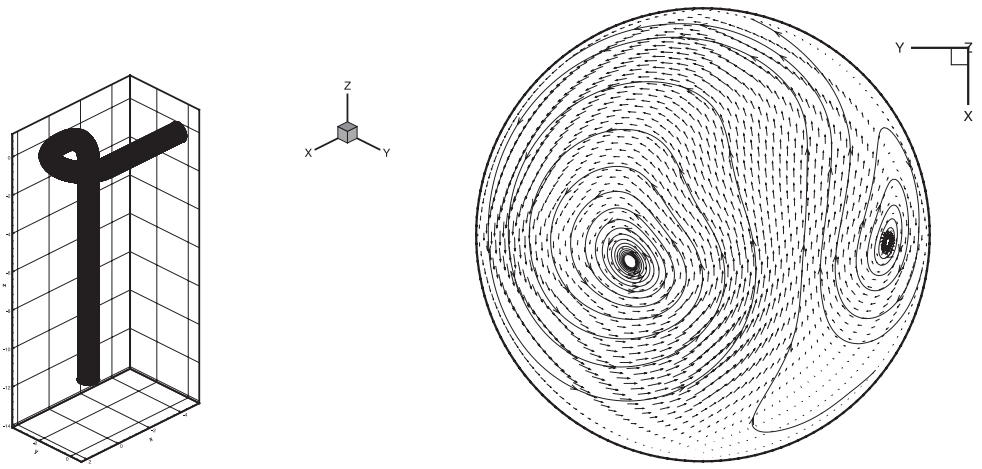


(a) (a)

Figure 5. (a) Grid of 90° arch. (b) Velocity distribution at the second outlet.

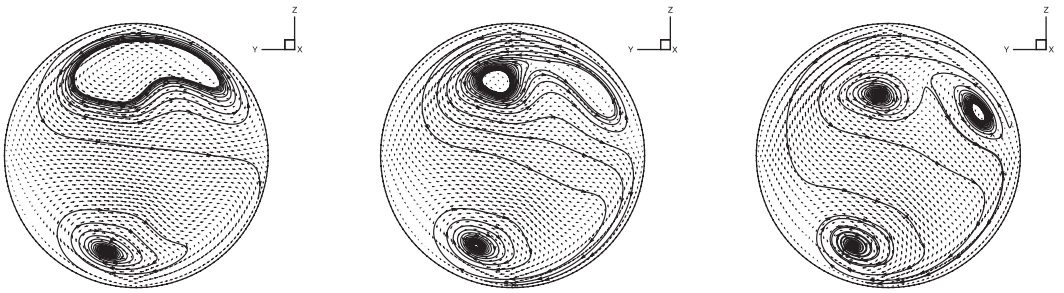

(a) (b) (c)

Figure 6. The history of vortices evolution in different sections of Kilner model. At (a) first outlet (b) between first outlet and second inlet, and (c) second inlet.

Figure 2 shows the velocity vectors in cross-section of the plane arch model at the first outlet. As expected the model shows the classical pair of counter-rotating vortices, Figure 3 shows the velocity vectors of the bi-curved plane arch at the second outlet. The flow structures change from one pair of counter-rotating to two pairs of counter vortices. The 45° arch model demonstrates an unsymmetic vortex pair in Figure 4. The kilner model shows the generation of a single helical vortex flow pattern (Figure 5). In this case, a single vortex accounts for approximately 90% of the cross sectional area. This result consists with the

 

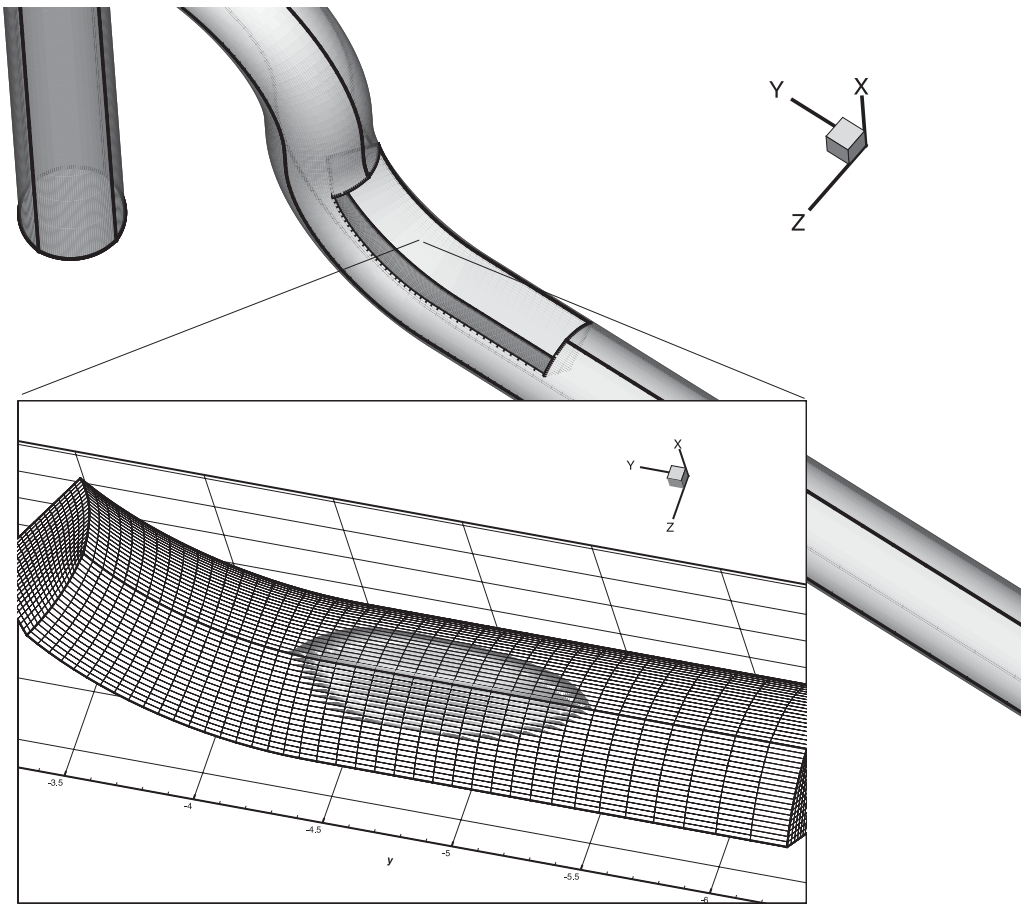


Figure 7. Region of separation in bi-curved arch.

result of Black *et al.* [3, Figure 4(b)]. Figure 6 shows the history of vortices evolution in different sections of Kilner model. Figure 6(a) is the first outlet of the arch. Figure 6(b) is the position between first outlet and second inlet. Figure 6(c) shows the velocity distribution at the second inlet. Figure 5(b) is at the second outlet. This shows how the helical vortex grows in the left lower-half region from Figure 6(c) to 5(b). Figures 7 and 8 show the regions of separation for the bi-curved plane and 45-degree arches. One can see that the region of separation of bi-curved arch is larger. The Kilner model shows no separation region. Figure 9 shows the swirl angles of three arches at their second outlet. The values of swirl angle of the Kilner arch are larger. This indicates that the strength of vortex in this model is stronger. Figure 10 shows the pressure histories of three arch models. One can see that the pressure drop among the bi-curved, 45°, and Kilner's arches, the drop of the Kilner model is the minimum.

 

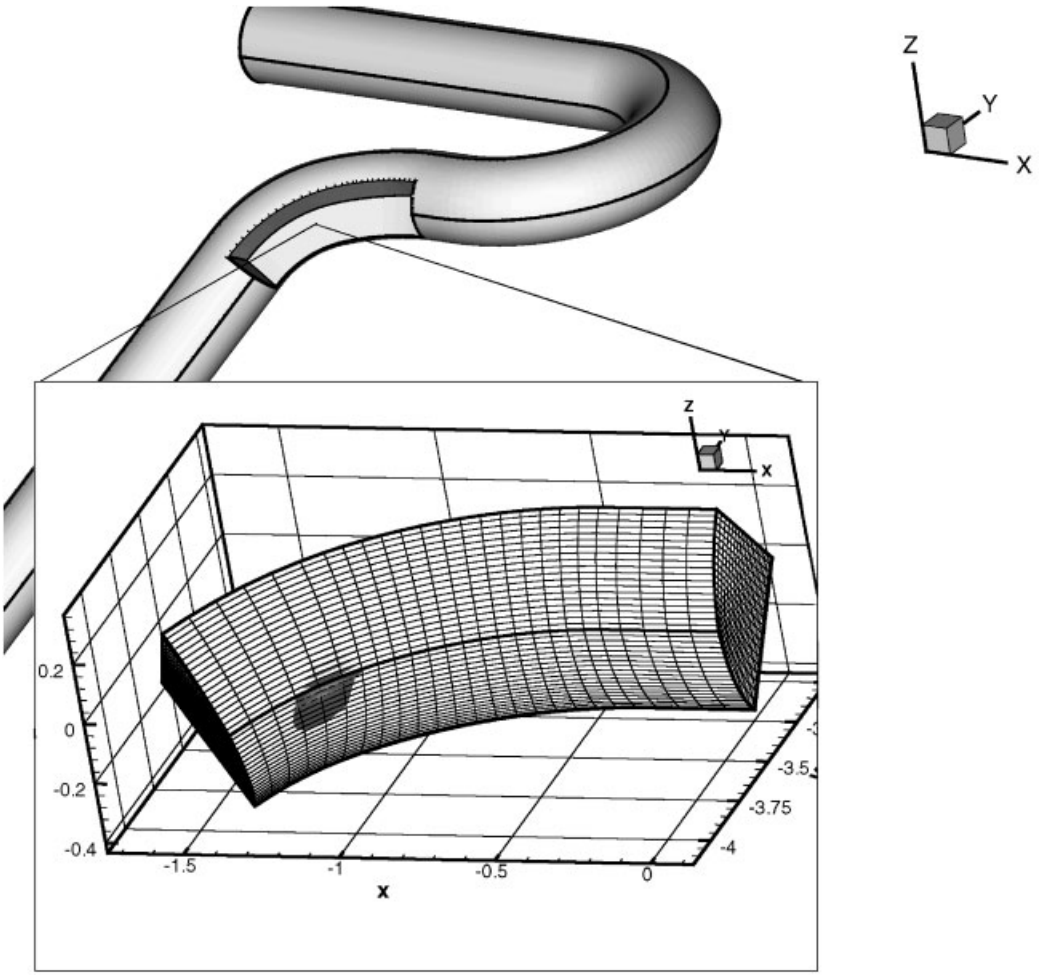


Figure 8. Region of separation in 45-degree arch.

## 5. CONCLUSIONS

An algorithm for computing steady-state and unsteady solutions to the incompressible Navier–Stokes equation is presented. The artificial compressibility method allows the equations to be solved as a hyperbolic dominated system in pseudo time. The use of upwind difference makes the scheme stable. With the use of a DDADI time integration, the method can be run large time steps and achieves very fast convergence. Comparisons of the compute results with some analytic solutions show good agreement. The numerical results show that the method is about 2.5-order accuracy in space and 1.8-order accuracy in time. For the flow in the aortic arch, the Kilner's arch achieves smallest pressure drop and doesn't occur flow separation in the whole arch. On the other hand, the bi-curved plane arch gives larger pressure drop and exists a largest separation region around the second turning section.

 

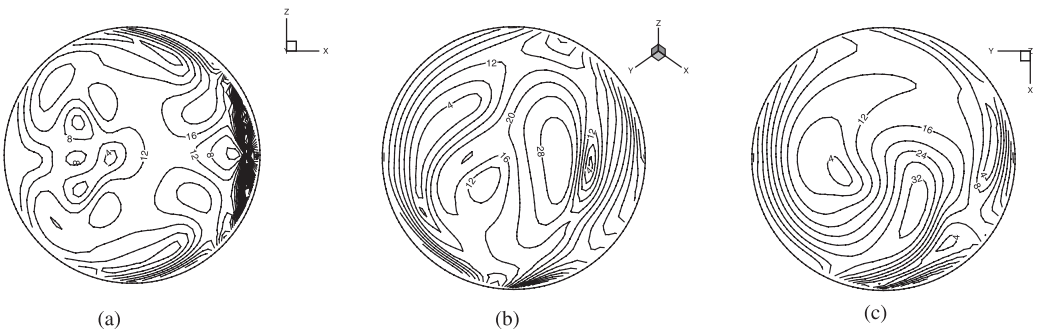


Figure 9. Swirl angles of three different arches: (a) bi-curved, (b) 45°, (c) Kilner arches.

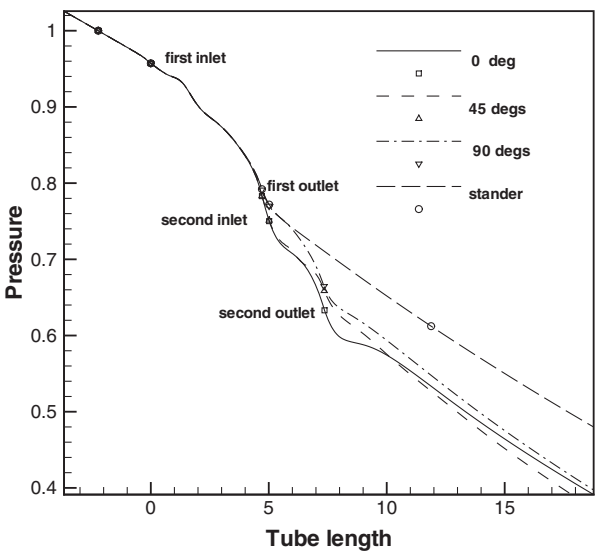


Figure 10. Pressure distribution vs tube length.

ACKNOWLEDGEMENTS

This works is partially supported by the National Science Council of the Republic of China under Contract NSC 89-2212-E-006-191.

REFERENCES

1. Yearwood TL, Chandran KB. Physiological pulsatile flow experiments in a model of the human aortic arch. *Journal of Biomechanics* 1984; **15**:683–704.
2. Kilner PJ, Young GZ, Mohaiddin RH, Firmin DN, Longmore DB. Helical and retrograde secondary flow patterns in the aortic arch studied by three directional magnetic resonance mapping. *Circulation* 1993; **88**(5):2235–2247.
3. Black MM, Hose DR, Lawford PV. The origin and signification of secondary flows in the aortic arch. *Journal of Medical Engineering Technology* 1995; **19**:192–197.
4. Chorin AJ. A numerical method for solving incompressible viscous flow problems. *Journal of Computational Physics* 1967; **2**:12–26.

 

5. Pan D, Chakravarthy SR. Unified Formulation for Incompressible Flows. *AIAA Paper 89-0122*, 1989.
6. Lin SY, Wu TM. An adaptive multigrid finite-volume scheme for incompressible Navier–Stokes equations. *International Journal of Numerical Methods in Fluids* 1993; **17**:687–710.
7. Klopher GH, Hung CM. A Diagonalized Diagonal Dominant Alternating Direction Implicit Scheme and Subiteration Correction. *AIAA Paper 98-2824*, 1998.
8. Yu ZX. Finite Volume Scheme for Incompressible Flows and its Applications to Internal and External Flows. *Ph.D. Thesis*, Department of Aeronautics and Astronautics, National Cheng Kung University, Tainan, Taiwan, 2002.
9. Ethier CR, Steinman DA. Exact fully 3D Navier–Stokes solutions for benchmarking. *International Journal of Numerical Methods in Fluids* 1994; **19**:369–375.

 